Applied Physics Letters

RESEARCH ARTICLE | APRIL 06 2026

Anisotropic dielectric function of graphite probed by far- and near-field spectroscopies

Adilet N. Toksumakov ; Georgy A. Ermolaev ; Dmitriy V. Grudinin; Aleksandr S. Slavich; Nikolay V. Pak ; Gleb V. Tikhonowski; Anton A. Minnekhanov ; Andrey A. Vyshnevyy ; Rodney S. Ruoff; Gleb I. Tselikov; Aleksey V. Arsenin; Valentyn S. Volkov

Appl. Phys. Lett. 128, 141902 (2026)
https://doi.org/10.1063/5.0320505

Applied Physics Letters ARTICLE pubs.aip.org/aip/apl

Anisotropic dielectric function of graphite probed by far- and near-field spectroscopies

Cite as: Appl. Phys. Lett. **128**, 141902 (2026); doi: 10.1063/5.0320505
Submitted: 31 December 2025 · Accepted: 16 March 2026 ·
Published Online: 6 April 2026

View Online Export Citation CrossMark

Adilet N. Toksumakov,[1] Georgy A. Ermolaev,[1] Dmitriy V. Grudinin,[1] Aleksandr S. Slavich,[1] Nikolay V. Pak,[1] Gleb V. Tikhonowski,[1] Anton A. Minnekhanov,[1] Andrey A. Vyshnevyy,[1] Rodney S. Ruoff,[2,3,4] Gleb I. Tselikov,[1] Aleksey V. Arsenin,[1] and Valentyn S. Volkov[1,a)]

AFFILIATIONS

[1]Emerging Technologies Research Center, XPANCEO, Internet City, Emmay Tower, Dubai, United Arab Emirates
[2]Center for Multidimensional Carbon Materials (CMCM), Institute for Basic Science (IBS), Ulsan, Republic of Korea
[3]Department of Chemistry, Ulsan National Institute of Science and Technology (UNIST), Ulsan, Republic of Korea
[4]Department of Materials Science and Engineering, Ulsan National Institute of Science and Technology (UNIST), Ulsan, Republic of Korea

[a)]Author to whom correspondence should be addressed: vsv@xpanceo.com

ABSTRACT

Graphite is a cornerstone material for novel technologies, from energy storage to two-dimensional materials. Despite its foundational role, the predictive power required for engineering emergent optical behavior in van der Waals heterostructures is severely constrained by persistent discrepancies in reported graphite optical constants. We resolve this long-standing ambiguity. A multi-modal approach synergizes far-field spectroscopic ellipsometry with nanoscale near-field optical probing (scattering-type scanning near-field optical microscopy) and micro-reflectance spectroscopy of graphite. We establish a new, self-consistent set of optical constants (n and k) for both in-plane and out-of-plane crystallographic directions across the ultraviolet-to-near-infrared spectrum. This definitive reference provides the essential foundation for the quantitative modeling and engineering of light–matter interactions in the evolving landscape of carbon-based nanophotonics.

Graphite, a crystalline allotrope of carbon, is defined by its highly anisotropic hexagonal layered structure composed of sp^2-hybridized carbon atoms arranged in two-dimensional graphene sheets.[1–3] These sheets are held together by weak van der Waals forces. The layered structure leads to a pronounced contrast in physical properties between the in-plane and out-of-plane directions. Such intrinsic anisotropy governs many of graphite's physical properties and is central to its technological relevance across diverse domains, ranging from classical applications such as lubricants and electrodes to modern uses in nanoelectronics, photonics, and optoelectronics—particularly following the advent of graphene[4] and other two-dimensional (2D) materials.[5,6] The advent of 2D materials opens new frontiers in nanophotonics and optoelectronics due to their unique properties, such as high refractive indices and strong optical anisotropy.[7–11]

Among the key descriptors of a material's interaction with electromagnetic radiation is its complex refractive index $n + ik$, where n is the standard refractive index (n) and k is the extinction coefficient (k). These quantities provide an insight into the material's electronic band structure and govern linear optical phenomena such as absorption, reflection, and transmission. The fundamental optical properties of bulk graphite have been shaped by seminal work after Taft and Philipp in 1965 (Ref. 12) which characterized its dielectric function by the contributions of π and σ electron transitions and identified a strong ultraviolet (UV) π-plasmon resonance.[13,14]

Since those early studies, the focus of the research community has shifted toward the optical effects observed in graphene, graphite's monolayer. Graphene exhibits a universal, frequency-independent optical absorption of ~2.3%[15,16] across the visible (VIS) and near-infrared (NIR) spectral range and allows for dynamic tuning of its properties via electrostatic gating,[17–20] making it an attractive material for applications in THz plasmonics and nonlinear optics.[21,22] Other van der Waals materials like transition metal dichalcogenides (TMDCs) have garnered attention because many of them undergo a transition from an indirect bandgap in bulk to a direct bandgap semiconductor as monolayers, enabling highly efficient light emission,[23–26] rich spin-valley physics,[27–29] and topological darkness biosensing.[30–32]

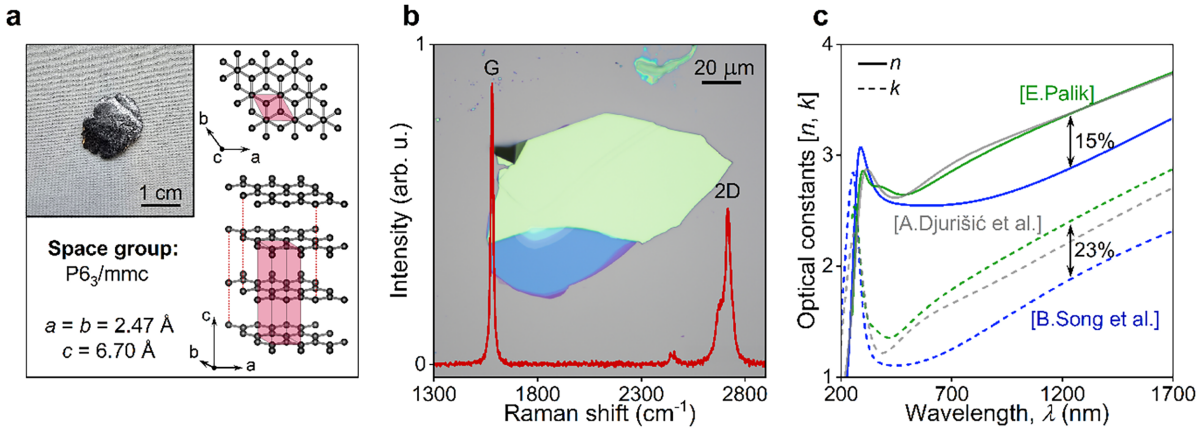

FIG. 1. Structure and optical properties of graphite. (a) Crystal structure of graphite. The inset represents an optical photo of bulk graphite. (b) Raman spectrum of graphite's flake. The optical micrograph of the flake is shown against a spectrum background. (c) Comparison of optical constants of graphite. Raw numerical data used for this graph were obtained from open access database[42] (available under the CC0 1.0 Universal Public Domain Dedication). Solid lines represent refractive index n; dashed lines represent extinction coefficient k.

Despite decades of research, a comprehensive and consistent dataset of graphite's anisotropic optical constants across a broad spectral range remains lacking, with considerable discrepancies in the literature[33–38] that frequently do not sufficiently account for differences in experimental techniques, sample quality, and data modeling strategies. Despite its foundational role, the predictive power required for engineering emergent optical behavior in van der Waals heterostructures is severely constrained by persistent discrepancies in reported graphite optical constants.

We report a comprehensive, high-accuracy determination of graphite's anisotropic optical constants over a wide spectral range (250–1700 nm) using a multi-technique approach. By combining spectroscopic ellipsometry with Raman spectroscopy for structural validation and near-field scanning optical microscopy (SNOM) and direct reflectance measurements of optical constants, we acquired a reference dataset of optical constants. Our work resolves long-standing inconsistencies and establishes a reliable foundation for modeling graphite-based components in advanced photonic, plasmonic, and optoelectronic systems, thereby reaffirming the relevance of this foundational material in the age of 2D photonics.

We began our investigation by characterizing the structural and vibrational properties of the bulk graphite source material (details in supplementary material Note 1). As a van der Waals crystal, graphite possesses a hexagonal layered structure (space group P6$_3$/mmc) with pronounced anisotropy, as depicted in Fig. 1(a). The crystalline quality of our samples was assessed via Raman spectroscopy performed on mechanically exfoliated flakes. The representative Raman spectrum in Fig. 1(b) exhibits the two characteristic fingerprints of high-quality crystalline graphite: an intense G peak at $\sim$1580 cm^{-1} arising from the in-plane sp^2 C–C bond vibrations, and a sharp 2D peak at $\sim$2720 cm^{-1}. The Lorentzian line shape of the 2D peak, along with the notable absence of the defect-activated D peak, indicates a low defect density and excellent three-dimensional crystalline order of our material, validating its suitability for precise optical measurements.[39–41] An optical micrograph of a measured graphite flake is presented in Fig. 1(b).

Before presenting our experimental results, it is crucial to contextualize the motivation for this study by visualizing the significant discrepancies present in the established literature. Figure 1(c) plots the in-plane optical constants, refractive index (n) and extinction coefficient (k), from several widely cited datasets.[33,34,36] While the overall spectral trends are qualitatively similar, quantitatively they diverge substantially. For instance, around the wavelength of 1200 nm, the reported values for the refractive index n differ by as much as 15%. The values for the extinction coefficient k, which dictates material loss, vary by up to 23% in the same spectral range.

These inconsistencies could present a significant obstacle to the design and predictive modeling of graphite-based photonic and optoelectronic devices. A new, consistent dataset is therefore required to address these discrepancies and provide a more accurate basis for future research and device engineering.

To address such inconsistencies, we performed variable-angle spectroscopic ellipsometry (SE), a powerful nondestructive technique that is exceptionally sensitive to the optical constants and anisotropy of materials. We measured the ellipsometric angles, Ψ (amplitude ratio) and Δ (phase difference) of reflected p- and s-polarized light, at four distinct angles of incidence (45°, 50°, 55°, and 60°) over a broad spectral range from 250 to 1700 nm [Figs. 2(a) and 2(b)]. The use of multiple incidence angles is critical, as it provides a set of independent measurements that over-determines the optical system, thereby allowing for the robust and unambiguous extraction of the anisotropic dielectric function.

The raw experimental data (Ψ and Δ) were analyzed using a detailed optical model. Given graphite's hexagonal crystal structure, it is optically described as a uniaxial material with its optical axis oriented along the crystallographic c-axis, perpendicular to the sample's layers. The complex dielectric function is therefore a tensor with two unique components: the in-plane ($\varepsilon_{||} = \varepsilon_{aa} = \varepsilon_{bb}$) and out-of-plane ($\varepsilon_{\perp} = \varepsilon_{cc}$) terms. The resulting real and imaginary parts of the complex dielectric function, $\varepsilon = \varepsilon_1 + i\varepsilon_2$ (or Re[ε] and Im[ε]), are presented in Figs. 2(c) and 2(d), respectively. These spectra reveal graphite's pronounced optical anisotropy. The dielectric function of

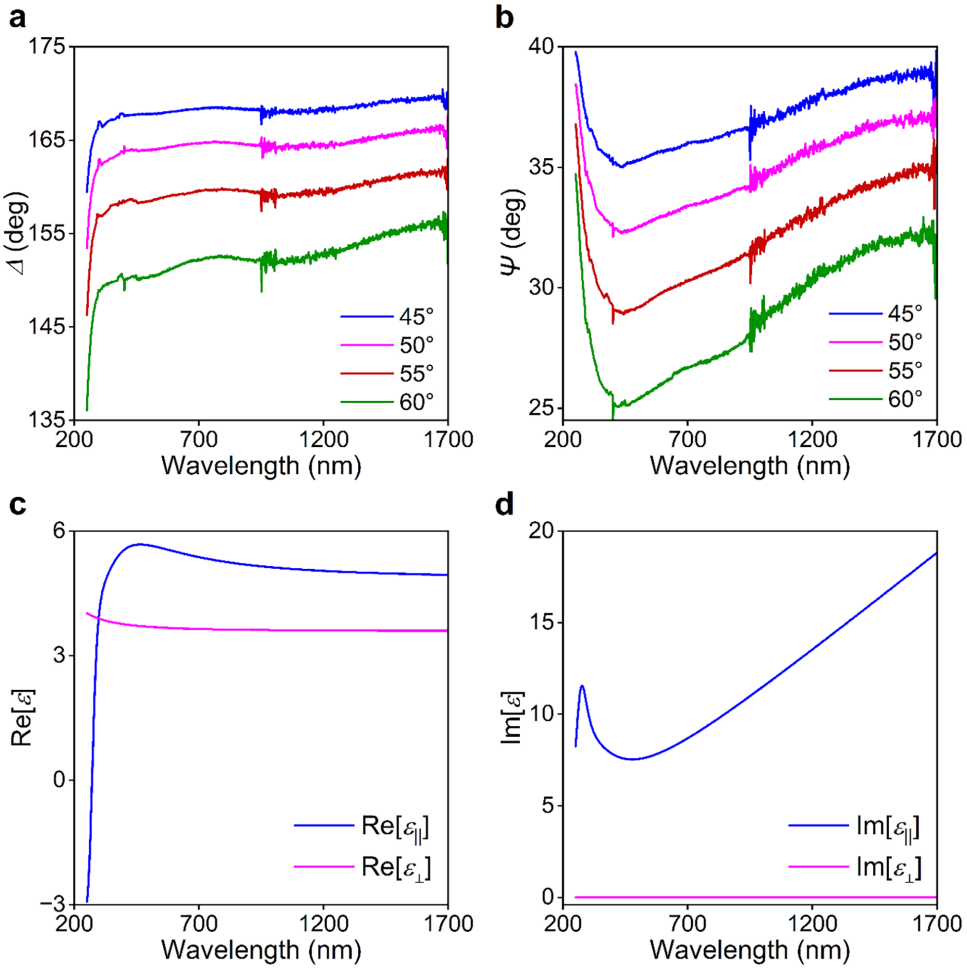

FIG. 2. Ellipsometric parameters: (a) Δ and (b) Ψ at incident angles 45°, 50°, 55°, and 60°. (c) Real and (d) imaginary parts of the dielectric function. The in-plane part is depicted by the blue line; the out-of-plane is presented by the magenta line.

graphite was parameterized using the Drude–Lorentz oscillators model (details in supplementary material Note 2).

The in-plane dielectric function ($\varepsilon_{||}$) is determined by the semimetallic electronic properties. Its imaginary part (Im[$\varepsilon_{||}$]), which represents optical absorption, is dominated by two key features. First, a prominent absorption peak is observed at approximately 280 nm, corresponding to the strong π–π^* interband transition.[43,44] Second, Im[$\varepsilon_{||}$] steadily increases toward longer wavelengths in the near-infrared scaling proportionally to the wavelength, which is the consequence of interband transitions near the Dirac cone.[12,45,46] The strong optical absorption at 280 nm leads via the causality to the abrupt changes in the real part (Re[$\varepsilon_{||}$]) in the UV range, so that it is negative in the ultraviolet region, crosses zero around 270 nm, and becomes positive at longer wavelengths. As a result, graphite behaves as a natural Type II hyperbolic material in the ultraviolet range (where Re[$\varepsilon_{||}$] < 0 and Re[$\varepsilon_{\perp}$] > 0), a feature relevant for engineering sub-diffractional light confinement and controlling the local density of optical states. This rich physics is accurately represented by the Kramers–Kronig-consistent dielectric function modeled with two Lorentz oscillators and the Drude term (supplementary material Note 2), although there is no significant free carrier contribution in the studied spectral range.

In contrast, the out-of-plane component ($\varepsilon_{\perp}$) displays a classic dielectric (insulating) response. The real part (Re[$\varepsilon_{\perp}$]) is positive and nearly constant at ∼3.6 across the entire spectral range. Correspondingly, the imaginary part (Im[$\varepsilon_{\perp}$]) is essentially zero, indicating negligible absorption along the *c*-axis. This extreme anisotropy is a direct consequence of graphite's electronic structure: the high in-plane conductivity is due to the mobile π electrons, while the weak van der Waals forces between layers effectively confine electrons within the planes, leading to insulating behavior in the out-of-plane direction. The self-consistent determination of these two distinct components provides the fundamental basis for accurately calculating the optical constants *n* and *k* and resolving the discrepancies found in the literature.

The dielectric function (ε) directly relates to the material's optical constants describing light propagation, the refractive index (*n*) and the extinction coefficient (*k*), as $\sqrt{\varepsilon} = n + ik$. For interactions with light at or near normal incidence, the response is dominated by the in-plane component of the dielectric tensor. Accordingly, we derived the in-plane optical constants ($n_{||}$ and $k_{||}$) from our experimentally determined dielectric function [Figs. 2(c) and 2(d)].

The results are presented in Fig. 3, where they are compared to two of the widely referenced datasets in the literature[33,34,36]

(comparison with more literature data in supplementary material Note 3). Our values for the refractive index ($n_{||}$) are plotted in Fig. 3(a). The spectrum is characterized by a value of ∼2.7 in the green visible region (∼550 nm), followed by a monotonic increase into the near infrared. While the seminal works of Palik[36] and Djurišić and Li[33] provide a reasonable approximation, our results are systematically lower across the entire spectral range. Conversely, the dataset from Song *et al.*[34] appears to significantly underestimate $n_{||}$, particularly at longer wavelengths. Our values address the discrepancy in the existing literature and are situated between the values reported in these prior studies.

A similar analysis for the extinction coefficient ($k_{||}$) is shown in Fig. 3(b). The spectrum for $k_{||}$ clearly reproduces the features discussed previously in the context of $\mathrm{Im}[\varepsilon_{||}]$: the extinction coefficient is characterized by a sharp peak near 250 nm. This feature is the manifestation of the π–π^* interband transition, which corresponds to the peak in the fundamental absorption $\mathrm{Im}[\varepsilon]$ at ∼280 nm. The shift in the peak position between k and $\mathrm{Im}[\varepsilon]$ is an expected consequence of the Kramers–Kronig relations. The shift occurs because the imaginary part of the dielectric function is related to the optical constants as $\mathrm{Im}[\varepsilon] = 2nk$. Since the real refractive index n is also frequency-dependent, the maximum of $2nk$ does not coincide with the maximum of k. Then, this peak is followed by the subsequent rise in the NIR arising due to interband transitions between the electronic states in the Dirac cones. Our data for k show good agreement with Palik's values in the UV-visible region and Djurišić and Li's in the NIR. The data from Song *et al.* deviate significantly, predicting much weaker absorption across most of the spectrum. These quantitative discrepancies underscore the need for a reevaluation of graphite's optical properties.

To independently verify the accuracy of our ellipsometry-derived dataset, we performed a direct normal incidence reflectance measurement on the same sample [Fig. 3(c)]. This provides a crucial cross-validation, as reflectance is a direct measure of light intensity and does not rely on the same modeling procedures as ellipsometry. We then used our newly determined n and k values from ellipsometry to calculate the expected reflectance spectrum (R) using the Fresnel equations. As shown in Fig. 3(c), the calculated spectrum is in excellent agreement with the directly measured experimental spectrum. This strong correspondence between results from these two independent optical methods provides confirmation of the accuracy and self-consistency of our determined optical constants, establishing them as a reliable benchmark for future optical design and fundamental studies.

To further test the optical constants obtained by ellipsometry and probe graphite's local optical response, we performed scattering-type scanning near-field optical microscopy (s-SNOM) in reflection geometry with pseudo-heterodyne detection [Fig. 4(a)]. This configuration enables simultaneous measurement of amplitude and phase of the scattered field. Illumination and collection were achieved with a parabolic mirror under oblique incidence, and the signal was demodulated at the third harmonic of the tip oscillation to isolate the genuine near-field contribution.

We performed near-field imaging on graphite flakes exfoliated onto CaF_2 substrates [Fig. 4(b)] using infrared excitation (1475–1600 nm). The complex near-field signal (amplitude and phase) from graphite was normalized to that of the CaF_2 substrate [Fig. 4(c)]. In this configuration, the near-field interaction is predominantly governed by the out-of-plane dielectric function ($\varepsilon_\perp$), particularly for highly anisotropic materials like graphite.

Measurements were conducted on two graphite flakes of 150 and 350 nm thickness exfoliated on CaF_2 substrates. The sample was illuminated by a tunable laser spanning 1475–1600 nm in 25 nm steps. Each scan included both flake and substrate areas, allowing point-by-point normalization of the complex near-field signal to the CaF_2 reference, thereby eliminating instrumental and tip-dependent factors.

Amplitude and phase images were recorded simultaneously [Fig. 4(c)]. The complex near-field signal from graphite was normalized to the response of the CaF_2 substrate within each scan. The normalized complex ratio

$$s_{\mathrm{rel}} = \frac{s_{\mathrm{graphite}}}{s_{\mathrm{CaF_2}}}$$

was analyzed using a dipole-interaction model in which the tip is treated as a metallic sphere interacting electrostatically with the sample.[47] The model parameters correspond to the experimental probe geometry and the optical properties of platinum. The complex permittivity of graphite was numerically retrieved by fitting the modeled and measured s_{rel} (details in supplementary material Note 4).

These s-SNOM results are in excellent agreement with the out-of-plane optical constants acquired independently from the far-field

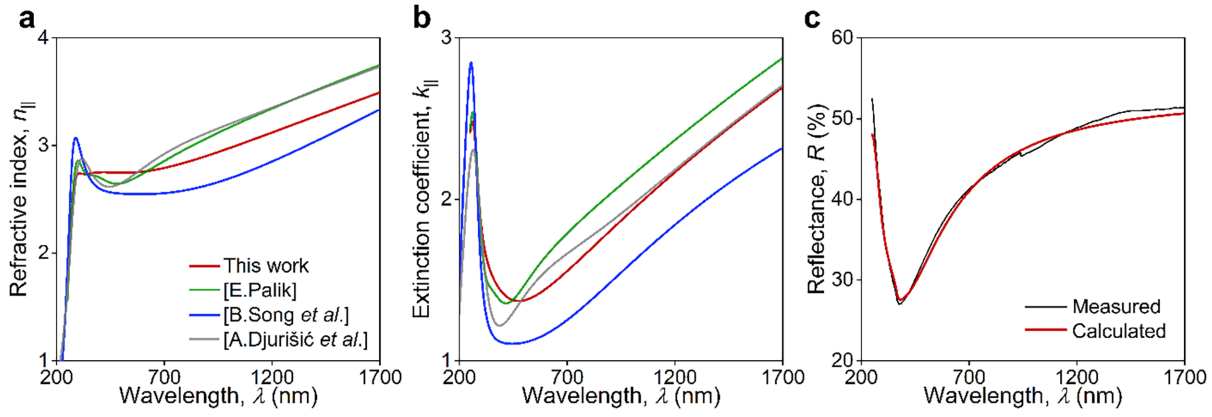

FIG. 3. Comparison of graphite's optical constants: (a) refractive index and (b) extinction coefficient. (c) Measured and calculated reflectance spectra.

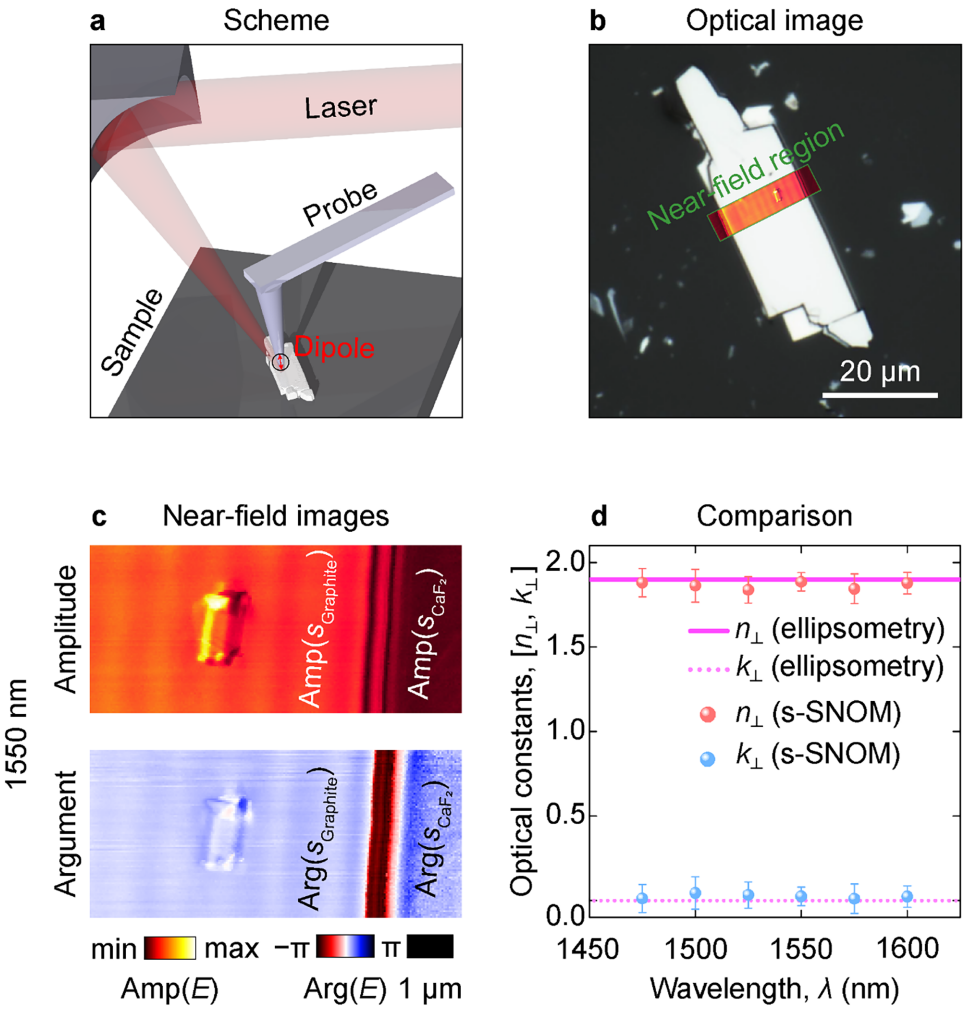

FIG. 4. Near-field extraction of graphite optical constants. (a) Schematic of the reflection-mode s-SNOM experiment. A focused infrared beam is directed and collected by the same parabolic mirror, illuminating a Pt-coated AFM probe that interacts with the sample through a nanoscale dipole field. (b) Optical micrograph of a graphite flake on a CaF_2 substrate showing the areas used for atomic-force (AFM) topography and near-field mapping. (c) Representative near-field amplitude (top) and phase (bottom) images acquired at $\lambda = 1550$ nm. The graphite region exhibits pronounced amplitude enhancement and phase shift relative to the CaF_2 substrate, corresponding to differences in local optical response. (d) Spectral dependence of the refractive index $n_\perp$ and extinction coefficient $k_\perp$ of graphite obtained from the near-field inversion (symbols) compared with ellipsometry (solid lines).

ellipsometry [solid lines in Fig. 4(d)]. Because the extraction of both in-plane ($\varepsilon_{||}$) and out-of-plane ($\varepsilon_\perp$) components from variable-angle ellipsometry is intrinsically coupled within the uniaxial model, this nanoscale validation of $\varepsilon_\perp$ provides strong corroboration for the accuracy and self-consistency of the entire anisotropic dielectric tensor determined in this work. This demonstrates that the macroscopic optical model accurately describes the material's response down to the nanometer length scale.

To put graphite's optical properties in context, we performed a comparative analysis of its optical constants against those of few-layer graphene (Fig. 5) and validated them via Raman spectroscopy and AFM (details in supplementary material Note 5). The optical constants, the refractive index and the extinction coefficient, for bulk graphite and 1-, 2-, and 3-layered graphene are presented in Figs. 5(a) and 5(b) (details in supplementary material Note 6). We also show in Fig. 5(c) the per-layer absorption. In the 2D limit, monolayer graphene exhibits a remarkable frequency-independent optical conductivity, leading to a universal absorbance $A = \pi\alpha \approx 2.3\%$,[15,16,48–50] a value dictated by the fine-structure constant (α). As layers are added, the interlayer coupling modifies the electronic band structure. This electronic evolution is directly reflected in the optical constants [Figs. 5(a) and 5(b)]. We observe a systematic increase in both the refractive index and the extinction coefficient with increasing thickness. This trend indicates a renormalization of the electronic structure and enhanced overall oscillator strength as the system evolves toward the bulk limit. Tabulated optical constants are presented in supplementary material Note 7.

Analyzing the per-layer absorption [Fig. 5(c)] provides insight into this dimensional crossover. While 1L graphene adheres closely to the universal value $\pi\alpha$ at longer wavelengths, few-layer graphene and bulk graphite exhibit a convergent behavior in the NIR. However, significant deviations emerge in the UV region, around the π–π^* transition. The per-layer absorption in bulk graphite is substantially enhanced compared to monolayer graphene in this spectral region. This enhancement highlights the influence of interlayer interactions and the evolving dimensionality on the collective electronic excitations, underscoring that the optical identity of graphite is distinct from a simple superposition of independent graphene layers.

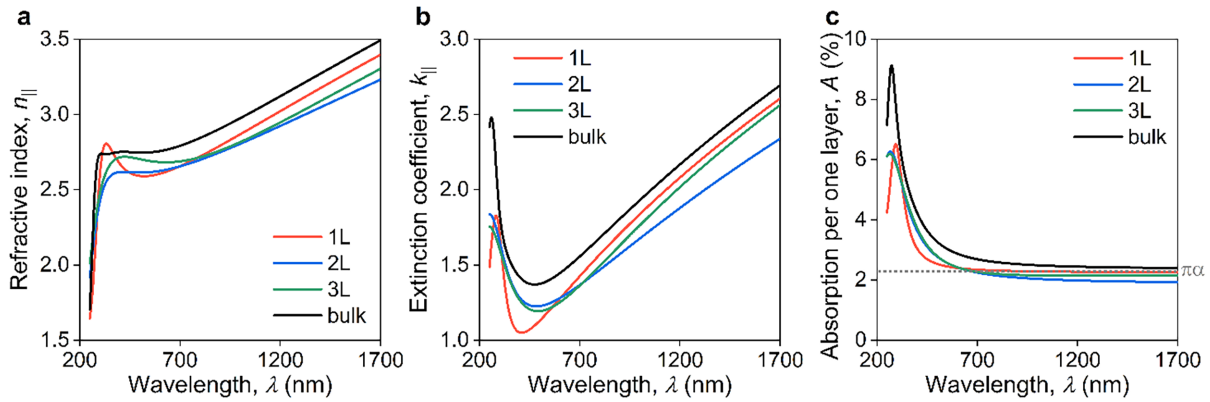

FIG. 5. Optical constants of graphite and 1-, 2-, and 3-layered graphene: (a) refractive index and (b) extinction coefficient. (c) Intrinsic absorbance of graphene.

In conclusion, we have established an accurate, self-consistent dataset for the anisotropic optical constants of bulk graphite. Derived from spectroscopic ellipsometry, these constants are cross-validated by independent micro-reflection spectroscopy and nanoscale near-field measurements, ensuring consistency from macroscopic to nanometer length scales. This multi-technique approach provides a new benchmark and resolves long-standing discrepancies in the literature.

This validated dataset provides the necessary foundation for the high-fidelity design of advanced photonic architectures harnessing the anisotropy of graphite, including hyperbolic metasurfaces, polarization-sensitive photodetectors, and complex van der Waals heterostructures, thereby removing uncertainty in simulations. By establishing graphite as a predictable and reliable nanophotonic platform, our work opens a direct path to accelerating the design and implementation of next-generation optical components.

See the supplementary material for materials and methods, additional figures, and tabulated optical constants.

The authors thank Dr. Alexey Tsapenko for help in measurements. R.S.R. was supported by the Institute for Basic Science (No. IBS-R019-D1).

AUTHOR DECLARATIONS

Conflict of Interest

The authors have no conflicts to disclose.

Author Contributions

Adilet N. Toksumakov, Georgy A. Ermolaev, and Dmitriy V. Grudinin contributed equally to this paper.

Adilet N. Toksumakov: Conceptualization (equal); Formal analysis (equal); Investigation (equal); Methodology (equal); Validation (equal); Visualization (equal); Writing – original draft (equal); Writing – review & editing (equal). **Georgy A. Ermolaev:** Conceptualization (equal); Formal analysis (equal); Investigation (equal); Methodology (equal); Validation (equal); Writing – original draft (equal); Writing – review & editing (equal). **Dmitriy V. Grudinin:** Investigation (equal); Methodology (equal); Validation (equal); Visualization (equal); Writing – review & editing (equal). **Aleksandr S. Slavich:** Investigation (equal); Writing – review & editing (equal). **Nikolay V. Pak:** Investigation (equal); Writing – review & editing (equal). **Gleb V. Tikhonowski:** Investigation (equal); Writing – review & editing (equal). **Anton A. Minnekhanov:** Investigation (equal); Writing – review & editing (equal). **Andrey A. Vyshnevyy:** Conceptualization (equal); Supervision (equal); Writing – review & editing (equal). **Rodney S. Ruoff:** Conceptualization (equal); Supervision (equal); Writing – review & editing (equal). **Gleb I. Tselikov:** Conceptualization (equal); Supervision (equal); Writing – review & editing (equal). **Aleksey V. Arsenin:** Conceptualization (equal); Supervision (equal); Writing – review & editing (equal). **Valentyn S. Volkov:** Conceptualization (equal); Supervision (equal); Writing – review & editing (equal).

DATA AVAILABILITY

The data that support the findings of this study are available from the corresponding author upon reasonable request.

REFERENCES

[1]J. D. Bernal, "The structure of graphite," Proc. R. Soc. London, Ser. A **106**, 749–773 (1924).
[2]A. N. Popova, "Crystallographic analysis of graphite by X-ray diffraction," Coke Chem. **60**, 361–365 (2017).
[3]S. Stankovich, D. A. Dikin, G. H. B. Dommett, K. M. Kohlhaas, E. J. Zimney, E. A. Stach, R. D. Piner, S. T. Nguyen, and R. S. Ruoff, "Graphene-based composite materials," Nature **442**, 282–286 (2006).
[4]K. S. Novoselov, A. K. Geim, S. V. Morozov, D. Jiang, Y. Zhang, S. V. Dubonos, I. V. Grigorieva, and A. A. Firsov, "Electric field effect in atomically thin carbon films," Science **306**, 666–669 (2004).
[5]K. S. Novoselov, D. Jiang, F. Schedin, T. J. Booth, V. V. Khotkevich, S. V. Morozov, and A. K. Geim, "Two-dimensional atomic crystals," Proc. Natl. Acad. Sci. U. S. A. **102**, 10451–10453 (2005).
[6]K. S. Novoselov, A. Mishchenko, A. Carvalho, and A. H. Castro Neto, "2D materials and van der Waals heterostructures," Science **353**, aac9439 (2016).
[7]G. A. Ermolaev, D. V. Grudinin, Y. V. Stebunov, K. V. Voronin, V. G. Kravets, J. Duan, A. B. Mazitov, G. I. Tselikov, A. Bylinkin, D. I. Yakubovsky, S. M. Novikov, D. G. Baranov, A. Y. Nikitin, I. A. Kruglov, T. Shegai, P. Alonso-González, A. N. Grigorenko, A. V. Arsenin, K. S. Novoselov, and V. S. Volkov, "Giant optical anisotropy in transition metal dichalcogenides for next-generation photonics," Nat. Commun. **12**, 854 (2021).

[8]D. V. Grudinin, G. A. Ermolaev, D. G. Baranov, A. N. Toksumakov, K. V. Voronin, A. S. Slavich, A. A. Vyshnevyy, A. B. Mazitov, I. A. Kruglov, D. A. Ghazaryan, A. V. Arsenin, K. S. Novoselov, and V. S. Volkov, "Hexagonal boron nitride nanophotonics: A record-breaking material for the ultraviolet and visible spectral ranges," Mater. Horiz. **10**, 2427–2435 (2023).
[9]S. Niu, G. Joe, H. Zhao, Y. Zhou, T. Orvis, H. Huyan, J. Salman, K. Mahalingam, B. Urwin, J. Wu, Y. Liu, T. E. Tiwald, S. B. Cronin, B. M. Howe, M. Mecklenburg, R. Haiges, D. J. Singh, H. Wang, M. A. Kats, and J. Ravichandran, "Giant optical anisotropy in a quasi-one-dimensional crystal," Nat. Photonics **12**, 392–396 (2018).
[10]A. S. Slavich, G. A. Ermolaev, M. K. Tatmyshevskiy, A. N. Toksumakov, O. G. Matveeva, D. V. Grudinin, K. V. Voronin, A. Mazitov, K. V. Kravtsov, A. V. Syuy, D. M. Tsymbarenko, M. S. Mironov, S. M. Novikov, I. Kruglov, D. A. Ghazaryan, A. A. Vyshnevyy, A. V. Arsenin, V. S. Volkov, and K. S. Novoselov, "Exploring van der Waals materials with high anisotropy: Geometrical and optical approaches," Light: Sci. Appl. **13**, 68 (2024).
[11]C. Cong, J. Shang, Y. Wang, and T. Yu, "Optical properties of 2D semiconductor WS_2," Adv. Opt. Mater. **6**, 1700767 (2018).
[12]E. A. Taft and H. R. Philipp, "Optical properties of graphite," Phys. Rev. **138**, A197–A202 (1965).
[13]M. F. Lin, C. S. Huang, and D. S. Chuu, "Plasmons in graphite and stage-1 graphite intercalation compounds," Phys. Rev. B **55**, 13961 (1997).
[14]L. Vitali, M. A. Schneider, K. Kern, L. Wirtz, and A. Rubio, "Phonon and plasmon excitation in inelastic electron tunneling spectroscopy of graphite," Phys. Rev. B **69**, 121414 (2004).
[15]R. R. Nair, P. Blake, A. N. Grigorenko, K. S. Novoselov, T. J. Booth, T. Stauber, N. M. R. Peres, and A. K. Geim, "Fine structure constant defines visual transparency of graphene," Science **320**, 1308–1308 (2008).
[16]A. N. Toksumakov, G. A. Ermolaev, M. K. Tatmyshevskiy, Y. A. Klishin, A. S. Slavich, I. V. Begichev, D. Stosic, D. I. Yakubovsky, D. G. Kvashnin, A. A. Vyshnevyy, A. V. Arsenin, V. S. Volkov, and D. A. Ghazaryan, "Anomalous optical response of graphene on hexagonal boron nitride substrates," Commun. Phys. **6**, 13 (2023).
[17]M. F. Craciun, S. Russo, M. Yamamoto, and S. Tarucha, "Tuneable electronic properties in graphene," Nano Today **6**, 42–60 (2011).
[18]J. Fernández-Rossier, J. J. Palacios, and L. Brey, "Electronic structure of gated graphene and graphene ribbons," Phys. Rev. B **75**, 205441 (2007).
[19]N. O. Weiss, H. Zhou, L. Liao, Y. Liu, S. Jiang, Y. Huang, and X. Duan, "Graphene: An emerging electronic material," Adv. Mater. **24**, 5782–5825 (2012).
[20]J. B. Oostinga, H. B. Heersche, X. Liu, A. F. Morpurgo, and L. M. K. Vandersypen, "Gate-induced insulating state in bilayer graphene devices," Nat. Mater. **7**, 151–157 (2008).
[21]A. N. Grigorenko, M. Polini, and K. S. Novoselov, "Graphene plasmonics," Nat. Photonics **6**, 749–758 (2012).
[22]T. Low and P. Avouris, "Graphene plasmonics for terahertz to mid-infrared applications," ACS Nano **8**, 1086–1101 (2014).
[23]K. F. Mak, C. Lee, J. Hone, J. Shan, and T. F. Heinz, "Atomically thin MoS_2: A new direct-gap semiconductor," Phys. Rev. Lett. **105**, 136805 (2010).
[24]A. Chaves, J. G. Azadani, H. Alsalman, D. R. da Costa, R. Frisenda, A. J. Chaves, S. H. Song, Y. D. Kim, D. He, J. Zhou, A. Castellanos-Gomez, F. M. Peeters, Z. Liu, C. L. Hinkle, S.-H. Oh, P. D. Ye, S. J. Koester, Y. H. Lee, P. Avouris, X. Wang, and T. Low, "Bandgap engineering of two-dimensional semiconductor materials," npj 2D Mater. Appl. **4**, 29 (2020).
[25]Z. Peng, X. Chen, Y. Fan, D. J. Srolovitz, and D. Lei, "Strain engineering of 2D semiconductors and graphene: From strain fields to band-structure tuning and photonic applications," Light: Sci. Appl. **9**, 190 (2020).
[26]P. G. Zotev, Y. Wang, D. Andres-Penares, T. Severs-Millard, S. Randerson, X. Hu, L. Sortino, C. Louca, M. Brotons-Gisbert, T. Huq, S. Vezzoli, R. Sapienza, T. F. Krauss, B. D. Gerardot, and A. I. Tartakovskii, "Van der Waals materials for applications in nanophotonics," Laser Photonics Rev. **17**, 2200957 (2023).
[27]D. Xiao, G. B. Liu, W. Feng, X. Xu, and W. Yao, "Coupled spin and valley physics in monolayers of MoS_2 and other group-VI dichalcogenides," Phys. Rev. Lett. **108**, 196802 (2012).
[28]E. S. Kadantsev and P. Hawrylak, "Electronic structure of a single MoS_2 monolayer," Solid State Commun. **152**, 909–913 (2012).
[29]A. Kormányos, G. Burkard, M. Gmitra, J. Fabian, V. Zólyomi, N. D. Drummond, and V. Fal'ko, "k·p theory for two-dimensional transition metal dichalcogenide semiconductors," 2D Mater. **2**, 022001 (2015).
[30]G. Ermolaev, K. Voronin, D. G. Baranov, V. Kravets, G. Tselikov, Y. Stebunov, D. Yakubovsky, S. Novikov, A. Vyshnevyy, A. Mazitov, I. Kruglov, S. Zhukov, R. Romanov, A. M. Markeev, A. Arsenin, K. S. Novoselov, A. N. Grigorenko, and V. Volkov, "Topological phase singularities in atomically thin high-refractive-index materials," Nat. Commun. **13**, 2049 (2022).
[31]V. Maslova, P. Lebedev, and D. G. Baranov, "Topological phase singularities in light reflection from non-Hermitian uniaxial media," Adv. Opt. Mater. **12**, 2303263 (2024).
[32]V. Maslova, G. Ermolaev, E. S. Andrianov, A. V. Arsenin, V. S. Volkov, and D. G. Baranov, "The influence of shot noise on the performance of phase singularity-based refractometric sensors," Nanophotonics **14**, 2463–2472 (2025).
[33]A. B. Djurišić and E. H. Li, "Optical properties of graphite," J. Appl. Phys. **85**, 7404–7410 (1999).
[34]B. Song, H. Gu, S. Zhu, H. Jiang, X. Chen, C. Zhang, and S. Liu, "Broadband optical properties of graphene and HOPG investigated by spectroscopic Mueller matrix ellipsometry," Appl. Surf. Sci. **439**, 1079–1087 (2018).
[35]D. L. Greenaway, G. Harbeke, F. Bassani, and E. Tosatti, "Anisotropy of the optical constants and the band structure of graphite," Phys. Rev. **178**, 1340–1348 (1969).
[36]E. D. Palik, *Handbook of Optical Constants of Solids* (Academic Press, 1997).
[37]R. Papoular, J. Breton, G. Gensterblum, I. Nenner, R. J. Papoular, and J.-J. Pireaux, "The vis/UV spectrum of coals and the interstellar extinction curve," Astron. Astrophys. **270**, L5–L8 (1993).
[38]T. Smausz, B. Kondász, T. Gera, T. Ajtai, N. Utry, M. Pintér, G. Kiss-Albert, J. Budai, Z. Bozóki, G. Szabó, and B. Hopp, "Determination of UV–visible–NIR absorption coefficient of graphite bulk using direct and indirect methods," Appl. Phys. A **123**, 633 (2017).
[39]S. Reich and C. Thomsen, "Raman spectroscopy of graphite," Philos. Trans. R. Soc. London, Ser. A **362**, 2271–2288 (2004).
[40]T. Tene, M. Guevara, A. Valarezo, O. Salguero, F. A. Arias, M. Arias, A. Scarcello, L. S. Caputi, and C. V. Gomez, "Drying-time study in graphene oxide," Nanomaterials **11**, 1035 (2021).
[41]R. Boroujerdi, A. Abdelkader, and R. Paul, "Highly sensitive and selective detection of the antidepressant amitriptyline using a functionalised graphene-based sensor," ChemNanoMat **8**, e202200209 (2022).
[42]M. N. Polyanskiy, see https://refractiveindex.info for "Refractive index database" (2016).
[43]A. G. Marinopoulos, L. Reining, A. Rubio, and V. Olevano, "*Ab initio* study of the optical absorption and wave-vector-dependent dielectric response of graphite," Phys. Rev. B **69**, 245419 (2004).
[44]M. K. Kinyanjui, C. Kramberger, T. Pichler, J. C. Meyer, P. Wachsmuth, G. Benner, and U. Kaiser, "Direct probe of linearly dispersing 2D interband plasmons in a free-standing graphene monolayer," Europhys. Lett. **97**, 57005 (2012).
[45]N. W. Ashcroft and N. D. Mermin, *Solid State Physics* (Holt, Rinehart and Winston, New York, 1976), Vol. 1.
[46]M. Fox, *Optical Properties of Solids* (Oxford University Press, 2010), Vol. 3.
[47]A. Cvitkovic, N. Ocelic, and R. Hillenbrand, "Analytical model for quantitative prediction of material contrasts in scattering-type near-field optical microscopy," Opt. Express **15**, 8550–8565 (2007).
[48]V. G. Kravets, A. N. Grigorenko, R. R. Nair, P. Blake, S. Anissimova, K. S. Novoselov, and A. K. Geim, "Spectroscopic ellipsometry of graphene and an exciton-shifted van Hove peak in absorption," Phys. Rev. B **81**, 155413 (2010).
[49]A. Matković, A. Beltaos, M. Milićević, U. Ralević, B. Vasić, D. Jovanović, and R. Gajić, "Spectroscopic imaging ellipsometry and Fano resonance modeling of graphene," J. Appl. Phys. **112**, 123523 (2012).
[50]J. W. Weber, V. E. Calado, and M. C. M. van de Sanden, "Optical constants of graphene measured by spectroscopic ellipsometry," Appl. Phys. Lett. **97**, 091904 (2010).